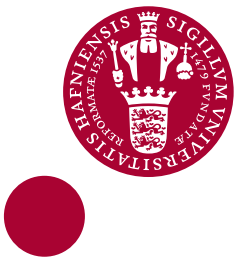

White Noise Background Improves Tone Discrimination by Suppressing Cortical Tuning Curves

Christensen, Rasmus Kordt; Linden, Henrik; Nakamura, Mari; Barkat, Tania Rinaldi

Published in:
Cell Reports

DOI:
10.1016/j.celrep.2019.10.049

Publication date:
2019

Document version
Publisher's PDF, also known as Version of record

Article

Cell Reports

White Noise Background Improves Tone Discrimination by Suppressing Cortical Tuning Curves

Graphical Abstract

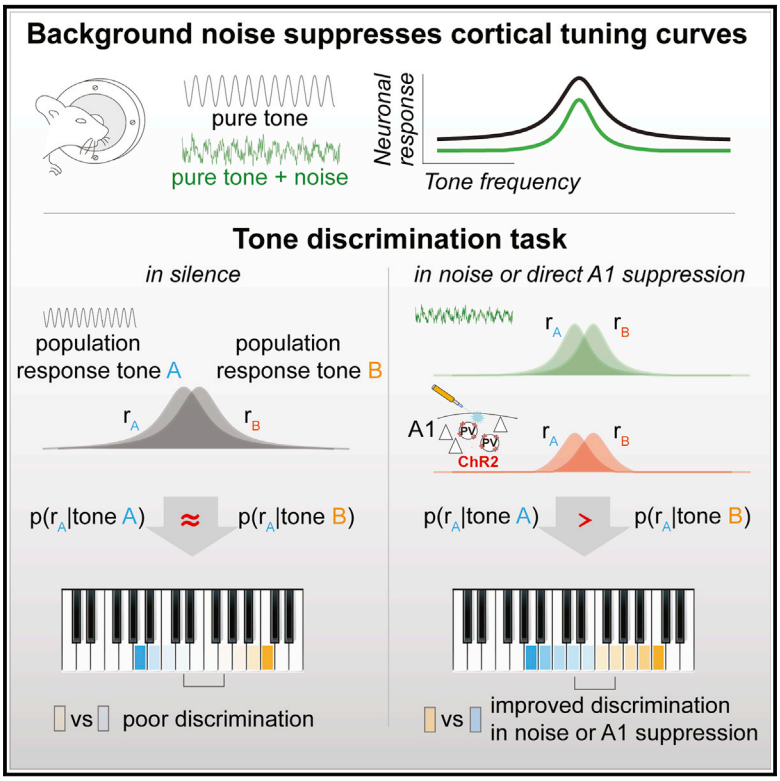

Highlights

- Background white noise suppresses tuning curves of auditory cortical neurons
- Background white noise increases the discriminability of spectrally similar tones
- PV$^+$ activation confirms the involvement of the cortex in the improved discriminability
- A population model links cortical activity suppression with behavioral improvement

Authors

Rasmus Kordt Christensen, Henrik Lindén, Mari Nakamura, Tania Rinaldi Barkat

Correspondence

tania.barkat@unibas.ch

In Brief

Christensen et al. ask how sensory representation and its perception change with noise. They show that background white noise suppresses the activity of A1 neurons, surprisingly increasing the discriminability of tones spectrally close to each other. Optogenetic manipulation of A1 confirms the involvement of this region in the behavioral improvement.

Christensen et al., 2019, Cell Reports *29*, 2041–2053
November 12, 2019
https://doi.org/10.1016/j.celrep.2019.10.049

CellPress

Cell Reports
Article

White Noise Background Improves Tone Discrimination by Suppressing Cortical Tuning Curves

Rasmus Kordt Christensen,[1,2,3] Henrik Lindén,[2] Mari Nakamura,[1] and Tania Rinaldi Barkat[1,4,*]
[1]Department of Biomedicine, Basel University, 4056 Basel, Switzerland
[2]Department of Neuroscience, University of Copenhagen, 2200 Copenhagen, Denmark
[3]Present address: Department of Physiology, Development and Neuroscience, University of Cambridge, Cambridge CB2 1TN, United Kingdom
[4]Lead Contact
*Correspondence: tania.barkat@unibas.ch
https://doi.org/10.1016/j.celrep.2019.10.049

SUMMARY

The brain faces the difficult task of maintaining a stable representation of key features of the outside world in noisy sensory surroundings. How does the sensory representation change with noise, and how does the brain make sense of it? We investigated the effect of background white noise (WN) on tuning properties of neurons in mouse A1 and its impact on discrimination performance in a go/no-go task. We find that WN suppresses the activity of A1 neurons, which surprisingly increases the discriminability of tones spectrally close to each other. To confirm the involvement of A1, we optogenetically excited parvalbumin-positive (PV^+) neurons in A1, which have similar effects as WN on both tuning properties and frequency discrimination. A population model suggests that the suppression of A1 tuning curves increases frequency selectivity and thereby improves discrimination. Our findings demonstrate that the cortical representation of pure tones adapts during noise to improve sensory acuity.

INTRODUCTION

Sensory processing is the basis of our interaction with the world and an essential part of brain function. At the cortical level, we know that neurons are informative about sensory inputs, as activity from cortical neurons can be decoded to reveal the stimulus inputs (Mesgarani et al., 2009; Rabinowitz et al., 2013; Klampfl et al., 2012). However, despite the successful decoding of sensory mapping, it is still unclear what sensory-related activity the brain uses for generating perceptions and goal-directed behavior.

Cortical neurons are typically responsive to only a subset of sensory features, implying a distributed sensory representation. A clear example of this is the auditory cortex, where specific neurons are selective to distinct sound frequencies. When presented with an auditory stimulus, the cortex receives spike trains resulting from activity in the cochlea. The cochlea deconstructs the external sound environment into frequency components (Von Bekesy, 1960), which are passed further along the auditory pathway up to the primary auditory cortex in a segregated manner (Guo et al., 2012; Hackett et al., 2011). This spatial separation of frequency components, conserved from the cochlea to the primary auditory cortex, is referred to as tonotopy (Evans et al., 1965; Goldstein et al., 1970). At the cellular level, tonotopy translates into spatially organized neurons with frequency-selective receptive fields. In many cases, these receptive fields are well characterized by a bell-shaped response to a varying stimulus, also referred to as a tuning curve. Auditory tuning curves are not, however, static; they have been shown to adapt during changes in stimulus context (Atiani et al., 2009; Reig et al., 2015) or attentional state (Carcea et al., 2017; Francis et al., 2018; Fritz et al., 2003), and it is believed that this flexibility is relevant for adjusting the dynamic range of sensory representation (Rabinowitz et al., 2013).

Embedding relevant sound features in background noise may also change tuning features. Previous studies in anesthetized animals have shown that background white noise (WN) introduces a threshold effect that lowers the response of cortical neurons to pure tone stimuli (Brugge et al., 1998; Ehret and Schreiner, 2000; Liang et al., 2014; Phillips, 1990; Zhou and Wang, 2010; Teschner et al., 2016). At the perceptual level, previous human psychophysics studies mostly reported a decrease in auditory saliency with noise (Martin et al., 1997; Whiting et al., 1998), but some showed a positive effect of noise on signal discrimination (Zeng et al., 2000) or speech perception (Kishon-Rabin et al., 2008). In animal models, where a direct correlation between neuronal activity and behavior would be possible, psychophysical experiments seeking to measure the limit of perception are more challenging. A recent study shows that sound location discrimination of a pure tone decreases gradually with signal to noise ratio (Sollini et al., 2016). It is unclear, however, how the threshold effect on tuning curves reported at the neuronal cortical level extends to animals in the awake state and how this suppression of activity influences the behavior of the animal.

A previous study confirms that the primary auditory cortex is directly involved in driving auditory perceptions and judgments during sensorimotor integration and behavior in a frequency-discrimination task (Aizenberg et al., 2015). Another study

indicates that changes in cortical neural population responses can alter behavioral performance (Briguglio et al., 2018). Also, the decoding of cortical activity confirms that the stimulus information needed for the categorization of sounds is present in A1 cortical neurons (Bathellier et al., 2012; Centanni et al., 2014). Despite this knowledge, we still have a poor understanding of how tuning curves are used by the brain to construct representations of auditory stimuli and how perturbations of these representations modify sensory-driven perceptions and related behaviors.

In the present study, we investigated the effect of WN on cortical tuning curves in awake mice and the behavioral relevance of the resulting tuning curve perturbations. During WN, we found a general suppression of tone-evoked activity in A1, in line with previous studies in anesthetized animals (Brugge et al., 1998; Ehret and Schreiner, 2000; Liang et al., 2014; Phillips, 1990; Zhou and Wang, 2010; Teschner et al., 2016). Associated with this suppression, we surprisingly found that WN improves discrimination performance for two tones with small frequency differences. We then asked whether the shift in cortical neuronal tuning properties is the underlying mechanism for this improved discriminability. Using optogenetics, we manipulated the neuronal response properties directly in A1 to mimic the tuning changes observed during our WN experiments and found that discriminability was improved for the same frequency range. Measurements in the auditory thalamus only weakly reflected the cortical tuning changes following the two perturbations. Finally, we used a simple model to illustrate how general suppression in tuned activity—as observed in A1 but not in thalamus—can lead to behavioral improvement in discrimination. Together, our results demonstrate that the tuning properties of A1 neurons are used by the brain to perform auditory discrimination and judgments relevant for stimulus-driven behavior.

RESULTS

WN Suppresses Responses to Pure Frequency Tones in A1

To investigate the stability of the representation of key features of an auditory stimulation in the presence of noise, we started by characterizing neural responses to pure frequency tones, perturbed it with a WN background, and determined whether this modification had any consequences at the behavioral level. Awake head-fixed mice were exposed to 37 randomly played pure frequency tones, spanning 3.7 octaves from 4 kHz to 48.7 kHz at 60 dB sound pressure level (SPL), lasting 50 ms each. Pure tones were presented in either a silent or continuous WN background at 50 dB SPL (referred to as no-WN or WN conditions, respectively). We recorded neuronal activity in the primary auditory cortex with multi-electrode arrays composed of four shafts with eight recording sites each. Voltage traces across the 32 channels were processed to extract single-unit (SU) activity (see STAR Methods).

Response characteristics of SUs were analyzed from the smoothed curve (see STAR Methods), obtained by plotting the mean spike rates (10 trials per stimulus) during sound stimulation as a function of the stimulus frequency (Figures 1A–1C). Each SU's preferred frequency was determined as the stimulus frequency evoking the peak spike rate of the smoothed curve. The peak spike rate was measured from the mean of the raw trial at the preferred frequency. The baseline spike rate was calculated as the median response spike rate for stimulus frequencies that elicited a spike rate lower than the mean spike rate of all stimulus frequencies. When comparing trials with no WN and those with WN, we found that peak spike rates were decreased ($peak_{noWN}$ = 29.3 ± 2.7 Hz; $peak_{WN}$ = 23.0 ± 1.9 Hz; N_{mice} = 10, n_{su} = 159; p = 0.0007; degrees of freedom [df] = 158; linear mixed model [LMM]) (Figure 1D). Baseline spike rates were also decreased ($baseline_{noWN}$ = 12.5 ± 1.5 Hz; $baseline_{WN}$ = 8.4 ± 1.0 Hz; N_{mice} = 10; n_{su} = 159; p = 0.0005; df = 158; LMM) (Figure 1E). These changes were observed across the whole tonotopic range (Figure S1A) and were not related to changes in preferred frequency (Figure S2A). We represented the overall change in tuning curves by aligning all responses to peak and calculating the grand mean (Figure 1F). WN produced a combined additive and multiplicative shift (Figure 1G; regression slope = 0.791; intersection = −1.53 Hz; r^2 = 0.97) corresponding to 26.1% suppression at peak and 14.2% suppression at baseline.

We then quantified frequency selectivity by measuring the percentage of stimulus frequencies tested giving a response with a spike rate at or above a threshold. The threshold was set at a fraction of each SU peak spike rate in each condition (no WN and WN). This percentage of frequencies represented at a threshold of 0.5 of the peak rate was significantly decreased (Figure 1H; percentage of freq. represented: $_{noWN}$ = 41.0% ± 2.1%; $_{WN}$ = 34.4% ± 1.8%; N_{mice} = 10; n_{su} = 159; p = 0.0004; df = 158; LMM), corresponding to an increased frequency selectivity with WN. The increased frequency selectivity was confirmed by a significant decrease in the sigma of the Gaussian fit on the subset of cells whose tuning curves could be approximated by a Gaussian distribution (see STAR Methods; Figure S3A; n_{su} = 27; p = 0.019; df = 26; LMM). Though more traditional, the method to estimate tuning width by measuring the sigma of the Gaussian fit does assume that tuning curves can be well fitted by a Gaussian function. This is the case for some SUs, but definitely not for all of them (27 out of 159 neurons in this case). The significant increase in frequency selectivity is, however, also observed in SUs that did not present a classical Gaussian tuning curve, as indicated by the less-conventional analysis method of frequency selectivity used here (Figure 1H).

As it is known that noise correlations may influence the ability of a population to code for sensory stimuli (Lin et al., 2015; Seriès et al., 2004), we next analyzed whether background WN influences inter-trial noise correlation. Noise correlation was only computed for trials with minimum spike rates above 1 Hz. Comparing no-WN to WN trials showed no significant difference (Figure 1I; n_{pairs} = 534; p = 0.187; df = 534; LMM). We also compared trial-by-trial variance, either as mean variance or variance normalized to mean spike rates (i.e., fano factor). The mean fano factor compared across all frequencies tested was unchanged (Figures 1J and 1K; $fano_{noWN}$ = 1.29 ± 0.03; $fano_{WN}$ = 1.35 ± 0.04; p = 0.151; df = 157; LMM). The average variance decreased with WN, as expected, since

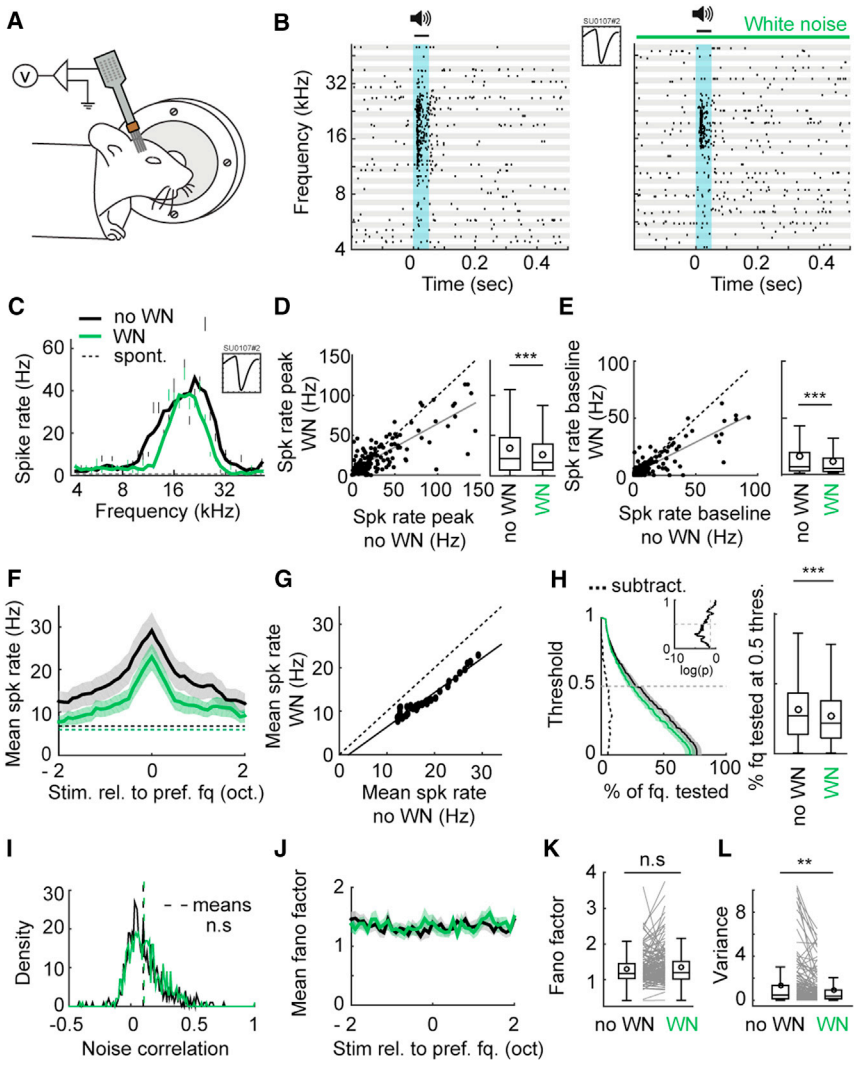

Figure 1. WN Suppresses Responses to Pure Frequency Tones in A1

(A) Schematic of experimental setup. An extracellular electrode is inserted into A1 of awake mice while pure tones are played in a silent or with-WN background.

(B) Example from a SU's raster plot of pure tone responses to 37 frequencies across 370 trials in no-WN and WN conditions.

(C) Same SU as in (B), with smoothed tuning curves plotted overlaying vertical lines of trial means ± SEM for each frequency tested. The dotted line indicates mean spontaneous activity during no WN.

(D and E) Scatterplot of peak spike rates (D) and baseline spike rates (E) in no-WN versus WN conditions for all SUs (n_{su} = 159; N_{mice} = 10). The dotted lines represent the unity lines, and the solid lines (gray) are the regression lines. Boxplots with mean spike rates (***p = 0.0007, ***p = 0.0005 for peak and baseline, respectively; LMM).

(F) Mean of peak-aligned tuning curves (n_{su} = 159; N_{mice} = 10). Shaded areas indicate 5%–95% confidence intervals. The dotted line represents mean spontaneous activity without WN.

(G) Mean tuning curves from (F) plotted against each other for all stimulus frequencies. The solid line indicates the regression line (slope = 0.791; intersection = −1.53 Hz; r^2 = 0.97).

(H) Means of cell-by-cell percentage of frequencies represented as a function of a normalized spike rate threshold. The dotted line is the subtraction of no-WN (black) and WN (green) lines. Boxplots with percentage of frequency represented at 0.5 of spike rate peak for no-WN and WN tuning curves (***p = 0.0004; LMM). Inset shows p values comparing no WN and WN for frequencies represented at all thresholds of peak-normalized tuning curves using Wilcoxon test. The vertical dotted line shows p = 0.05.

(I) Noise correlation between pairs of SUs within individual mice (n_{pairs} = 534; p = 0.187; df = 534; LMM).

(J) Fano factor of response to stimulus frequency relative to preferred frequency for all SUs.

(K and L) Mean fano factor (K) and trial-to-trial variance (L) across all frequencies (fano factor: p = 0.151, LMM; variance: **p = 0.0029, LMM). All boxplots show medians and 25th–75th and 10th–90th percentiles; circles indicate means.

See also Figures S1 and S2.

variance scales with the number of spikes (Figure 1L; $variance_{noWN}$ = 1.31 ± 0.17; $variance_{WN}$ = 0.90 ± 0.17; p = 0.0029; df = 158; LMM).

In summary, our findings show that background WN significantly suppresses responses to pure tone stimulation, both as peak and baseline spike rates, resulting in a negative shift of tuned responses of A1 neurons. Noise correlation and fano factor remain unaffected.

WN Improves Pure Tone Discrimination in a Frequency-Dependent Manner

How does such a mean suppression of spiking activity in auditory cortical neurons affect tone discrimination performance in mice? We tested the effect of background WN as mice performed a go/no-go discrimination task. The mice were trained to lick a drop of liquid in response to a pure frequency tone (go tone) and to restrain from licking when hearing another tone frequency (no-go tone). An incorrect lick was punished with a mild air puff and time out (Figure 2A). The mice learned the task in 3–6 days (Figures S4A and S4C). Once the task was learned, the difficulty of the task was increased by bringing the no-go tone closer in frequency to the go tone, until the animal was no longer able to discriminate between the tones (Figures S4A, S4B, and S4D). In this testing phase, the go tone was kept constant at 7 kHz, and the no-go tone was progressively shifted from 12 to 8 kHz in steps of 1 kHz (corresponding to frequency intervals of 0.8, 0.65, 0.5, 0.35, and 0.2 octaves between the go and no-go tones). Blocks of 100 trials with WN or no-WN backgrounds were tested in random order for each no-go tone (Figure S4B; see STAR Methods). The increasing difficulty of the task was reflected in a gradual decrease in the discriminability index

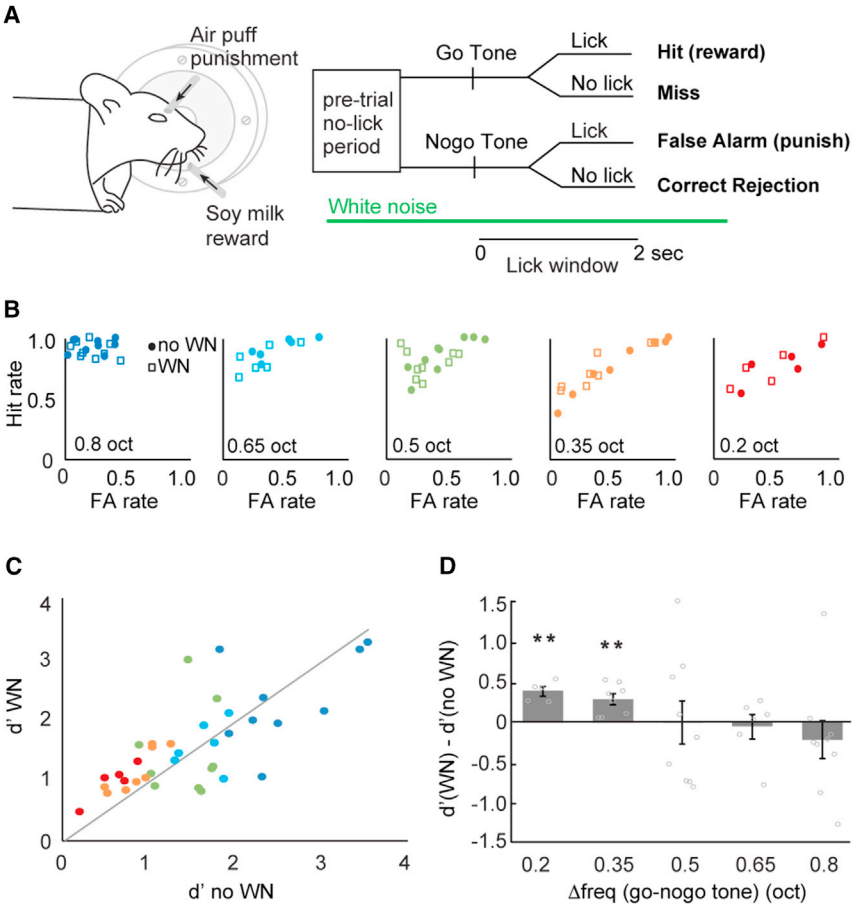

Figure 2. WN Improves Pure Tone Discrimination in a Frequency-Dependent Manner

(A) Schematic of auditory go/no-go discrimination task.

(B) Hit rate versus FA rate for no-WN (filled circles) and WN background (empty squares) for each go/no-go frequency interval. Each pair of filled circle and empty square represents a single mouse tested at different frequency intervals.

(C) Discriminability index d′ for WN versus no-WN conditions. The color code represents the frequency interval between the go and no-go tones, as in (B).

(D) Same data as in (C), but displayed as d′ changes with WN background (n = 5, 8, 9, 6, 9 mice; **p = 0.002, p = 0.001; paired t test). Data show mean ± SEM.

See also Figure S4.

d′ (Figure S4D). Switching the no-go tone to 0.8 octaves below the go tone (4 kHz) produced the same d′ as the no-go tone at 0.8 octaves above the go tone (Figure S4E). This implies that the discrimination difficulty is related to the distance in octave and not to the absolute frequencies. The decay in d′ is a result of a decreasing hit rate as well as increasing false alarm (FA) rate (Figures 2B and S4F), indicating that the increasing difficulty affects both go and no-go trials. A gradual decline in motivation due to increasing satiety during a session was not the cause of this decay, since d′ was back to its initial value at the end of the session (Figure S4G).

Including background WN significantly improved discrimination performance for frequency intervals of 0.35 (d'_{WN}-d'_{noWN} = 0.24 ± 0.07; n_{mice} = 8; p = 0.001; paired t test) and 0.2 octave (d'_{WN}-d'_{noWN} = 0.39 ± 0.05; n_{mice} = 5; p = 0.002; paired t test) but had no effect for larger frequency intervals (Figures 2C and 2D). Given that the reaction time from the tone onset to the lick was not affected by background WN (Figures S4H and S4I), this manipulation did not seem to affect the effectuation of motor-related programs.

These experiments lead to the counterintuitive observation that noise can improve auditory discrimination. In humans, it is clear that auditory acuity, like frequency discrimination (Henning, 1967) or speech recognition (Martin et al., 1997), can be impaired by noise. However, some studies have also shown that noise allows for smaller-frequency difference detection (Labiak and Wilson, 1974), increases auditory signals (Alain et al., 2009), or promotes acuity for certain signal-to-noise ratios (Javel et al., 1971; Kishon-Rabin et al., 2008; Zeng et al., 2000). To test whether the behavioral changes we observed are related to the changes in cortical tuning curves, and to address the possibility that WN may affect discrimination performance by mechanisms residing outside of A1 or by mechanisms that we did not consider to analyze, we next used optogenetics to selectively control the tuning curves of A1 neurons.

Light-Induced Activation of PV$^+$ Interneurons Modulates Frequency Tuning in the Auditory Cortex

It has been reported that specific activation of PV$^+$ cells can alter the tuning properties of sensory neurons. For example, PV photoactivation in the auditory cortex has been shown to decrease the magnitude of tone-evoked responses (Aizenberg et al., 2015; Hamilton et al., 2013) and to produce a mixture of divisive and subtractive suppression on both spontaneous and tone-evoked neuronal activities (Seybold et al., 2015). In order to specifically manipulate auditory cortical neuron responses, we expressed the light-sensitive cation channel, channelrhodopsin-2 (ChR2), in PV$^+$ interneurons using a breeding cre-lox approach (see STAR Methods). ChR2 was successfully expressed in the majority of PV$^+$ neurons in the auditory cortex, and all ChR2-positive neurons were positive for PV$^+$ (Figure S5A). We tested the light effect on auditory cortical spiking with cell-attached and intracellular recordings (Figure S5C). We found that the suppression in spiking activity of excitatory neurons caused by light-driven activation of PV$^+$ interneurons varied from mouse to mouse and was independent of cortical depth up to 800 μm below the pia surface (Figure S5E). We titrated

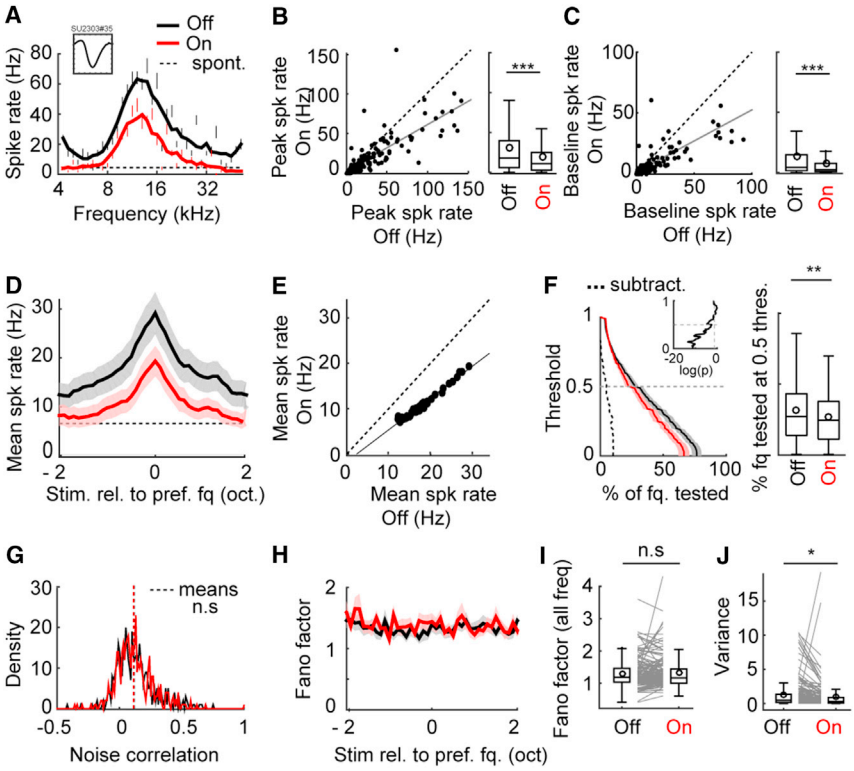

Figure 3. Light-Induced Activation of PV⁺ Interneurons Modulates Frequency Tuning in the Auditory Cortex

(A) Example of frequency-dependent spike rate responses in light-off (black) and light-on (red) conditions in a PV-ChR2 mouse, as recorded with extracellular electrophysiology. All lines and symbols are as indicated in Figure 1.

(B and C) Scatterplot of peak (B) and baseline (C) spike rates in light-off versus light-on conditions for all SUs (n_{su} = 159; N_{mice} = 10). Boxplots with mean spike rates (***p < 0.0005, p < 0.0005 for peak and baseline respectively; LMM).

(D) Mean of peak-aligned tuning curves (n_{su} = 159; N_{mice} = 10). The dotted line represents spontaneous activity. Shaded areas indicate 5%–95% confidence intervals.

(E) Mean tuning curves from (D) plotted against each other for all stimulus frequencies (regression line: slope = 0.701; intersection = −1.68 Hz; r^2 = 0.988).

(F) Means of cell-by-cell percentage of frequencies represented as a function of a normalized spike rate threshold. The dotted line is the subtraction of light-off (black) and light-on (red) lines. Boxplots with percentage of frequency represented at a threshold set at 0.5 fraction of peak spike rate for light-off and light-on tuning curves (**p = 0.0011; df = 158; LMM). Inset shows p values comparing light off and on for frequencies represented at all thresholds of peak-normalized tuning curves using Wilcoxon test. The vertical dotted line shows p = 0.05.

(G) Noise correlation between pairs of SUs within individual mice in light-off (black) and light-on (red) conditions (n_{pairs} = 452; p = 0.429; df = 451; LMM).

(H) Fano factor relative to preferred frequency for all SUs.

(I and J) Mean fano factor (I) and trial-to-trial variance (J) across all frequencies (fano factor: p = 0.382, LMM; variance: *p = 0.0265, LMM). All boxplots show medians and 25th–75th and 10th–90th percentiles; circles indicate means.

See also Figures S1–S3 and S5.

the light power in each mouse so that the sound-evoked peak response was inhibited to roughly 50% of its control amplitude (Figure S5D). This ensured a comparable level of inhibition across mice. The light pulse started at the tone onset and was maintained for the full duration of the tone (50 ms) to target the immediate tone representation in cortical circuits.

As previously described, we used extracellular electrophysiological recordings to measure tuned responses to different pure frequency tones. The preferred frequencies, peaks, and baseline spike rates were measured as described previously. As expected from the light titration approach, we observed that light activation of PV⁺ interneurons significantly decreased the peak spike rates (Figures 3A and 3B; $peak_{off}$ = 29.3 ± 2.6 Hz; $peak_{on}$ = 19.3 ± 1.9 Hz; N_{mice} = 10; n_{su} = 159; p < 0.0005; df = 158; LMM), as well as baseline spike rates (Figures 3A and 3C; $baseline_{off}$ = 12.8 ± 1.5 Hz; $baseline_{on}$ = 7.8 ± 1.2 Hz; N_{mice} = 10; n_{su} = 159; p < 0.0005; df = 158; LMM), independently of the preferred frequencies (Figure S1B). This was not related to a change in preferred frequency between both conditions (Figure S2A). As for the WN experiments, we plotted the mean of the tuning curves aligned to the peak (Figure 3D). PV⁺ perturbation produced a combined additive and multiplicative shift (regression slope = 0.701; intersection = −1.68 Hz; r^2 = 0.988) corresponding to a 35.6% suppression at peak and 18.8% suppression at baseline (Figure 3E). We also found an increase in frequency selectivity, as estimated by a reduction in the percentage of frequencies represented as a function of a threshold normalized to peak responses in each condition. Comparing the percentage of frequencies represented at a threshold of 0.5 of peak showed a significant reduction in light on trials (Figure 3F; percentage of freq. represented: $_{Off}$ = 41.0% ± 3.3%; $_{On}$ = 34.0% ± 3.5%; N_{mice} = 10; n_{su} = 159; p = 0.0011; df = 158; LMM). As for the WN perturbation, this increase in frequency selectivity could be confirmed by a significant decrease of sigma in the subset of cells whose tuning curves could be approximated by a Gaussian distribution (Figure S3B; n_{su} = 27; p = 0.0014; df = 26; LMM). Light-driven activation of PV⁺ neurons did not affect noise correlation (Figure 3G; n_{pairs} = 452; p = 0.429; df = 451; LMM). The mean fano factor was also unchanged (Figures 3H and 3I; $fano_{off}$, = 1.31 ± 0.06; $fano_{on}$, = 1.33 ± 0.01; p = 0.382; df = 157; LMM), while mean variance decreased due to the overall decrease in spike rates (Figure 3J; $variance_{off}$, = 1.31 ± 0.11; $variance_{on}$, = 0.95 ± 0.08; p = 0.0265; df = 158; LMM).

To look at a possible mechanistic relationship between the WN suppressive effect and PV⁺ neuron activity, we performed experiments combining a continuous WN background with light-induced activation of PV⁺ neurons with the same conditions described above. We found that combining both perturbations

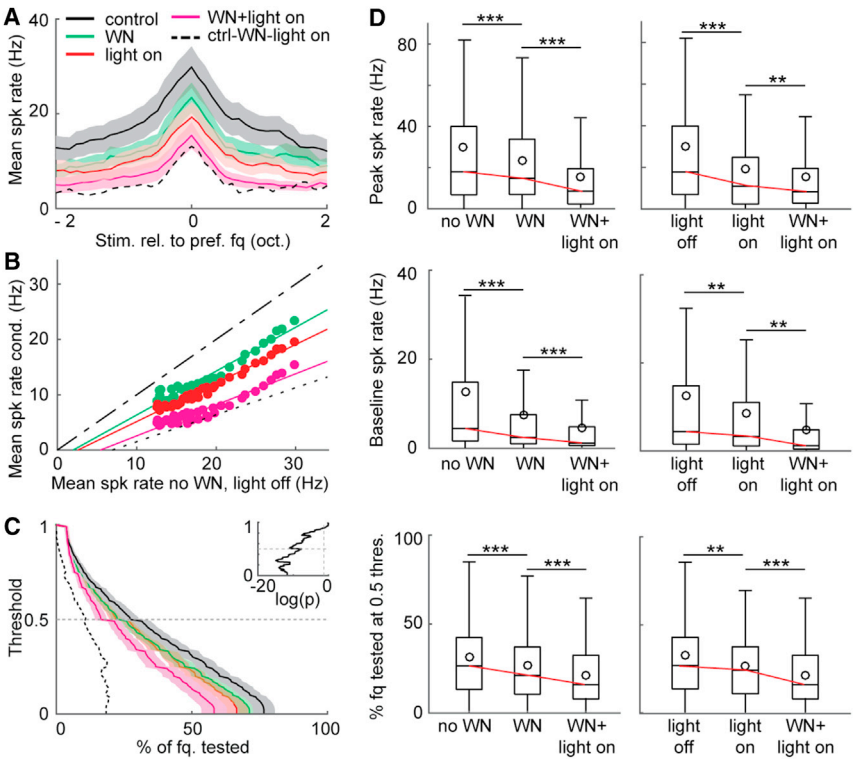

Figure 4. Continuous WN and PV Perturbations Have Additive Effects

(A) Mean of peak-aligned tuning curves (n_{su} = 159; N_{mice} = 10). Shaded areas indicate 5%–95% confidence intervals. The dotted line represents the additive effects of isolated WN and PV$^+$ neuron perturbation effects by subtracting them from the control curve.

(B) Mean tuning curves from (A) plotted against each other for all stimulus frequencies. The solid line indicates the regression lines. The dotted line represents the additive effects of isolated WN and PV$^+$ neuron perturbation effects by subtracting them from the control curve.

(C) Means of cell-by-cell percentage of frequencies represented as a function of a normalized spike rate threshold. The dotted line is the subtraction of control (black) and WN + light-on (pink) lines. Inset shows p values comparing control and WN + light on for frequencies represented at all thresholds of peak-normalized tuning curves using Wilcoxon test. The vertical dotted line shows p = 0.05.

(D) Boxplots comparing controls (no WN or light off), WN, or light on and WN + light on together (peak spike rate of WN versus WN + light on, ***p < 0.0001; light on versus WN + light on, **p = 0.0051; baseline spike rate WN versus WN + light on, ***p < 0.0003; light on versus WN + light on, **p = 0.0035; % frequency tested at 0.5 threshold WN versus WN + light on, ***p < 0.0001; light on versus WN + light on, ***p < 0.0001; LMM). Circles indicate means. Red lines mark the medians showing a near linear effect of combining continuous WN and PV$^+$ neuron perturbation.

resulted in a response suppression that was largely similar to the sum of the suppressive effects of WN and PV$^+$ neuron activation separately (Figure 4). These results indicate that the activation of cortical PV$^+$ neurons might not be the driving mechanism behind the suppressive effect induced by WN.

Given the large similarities in the representations of pure tones in A1 between background WN and light-induced changes, we asked whether PV$^+$ neuron activation improves discrimination performance in the same interval range as the background WN does.

Tone Discrimination Improves with Light Excitation of A1 PV$^+$ Interneurons

Using optogenetics, we tested the effect of light-driven activation of PV$^+$ neurons in the same go/no-go discrimination task described previously (Figure 5A). In these experiments, a craniotomy was performed to insert electrodes and set the light intensity to induce a suppression of roughly 50% in pure tone-evoked responses, similar to the passive recordings described above (Figures S6A and S6B). We found no difference in discrimination performance for pure tone intervals of 0.8, 0.65, and 0.5 octaves when comparing light-off versus light-on trials, while a significant improvement in performance was noted for the smaller intervals of 0.35 and 0.2 octaves (Figures 5B-5D; d'_{on}-d'_{off} = 0.42 ± 0.14; n_{mice} = 8; p = 0.021; d'_{on}-d'_{off} = 0.50 ± 0.12; n_{mice} = 6; p = 0.008, respectively; paired t test). As for the WN perturbations (Figure S4F), this improvement in discrimination performance was due to a decrease in FA rates (Figure S6E). We found no change in reaction time, suggesting that light-driven activation of PV$^+$ neurons does not impose changes in motor-related areas driving the behavior (Figures S6C and S6D). The light effect was not caused by retinotopic activation, as light did not alter the discrimination performance in control mice (Figure 5D).

Our results prove that activating PV$^+$ neurons suppresses tuned responses of A1 neurons similar to WN and enhances the discrimination performance for tones close in frequency in a similar range to WN. Together, the WN and optogenetic perturbations suggest that mice use the response features of A1 neurons to form perceptions and discriminate between pure tones. Although PV$^+$ neurons were targeted at the cortical level, thalamic neurons could be influenced by these cortical perturbations via cortico-thalamic projections (Guo et al., 2017), and behavioral performance could hence be explained by thalamic changes in activity. To address this possibility, we recorded in the auditory thalamus and tested the effect of the two perturbations.

Thalamic Responses Weakly Reflect Cortical Tuning Changes during WN and Light-Induced Activation of Cortical PV$^+$ Neurons

We asked how changes in cortical tuning properties imposed by WN or cortical PV$^+$ activation would reflect in the auditory thalamus. We used a linear multi-electrode array to reach

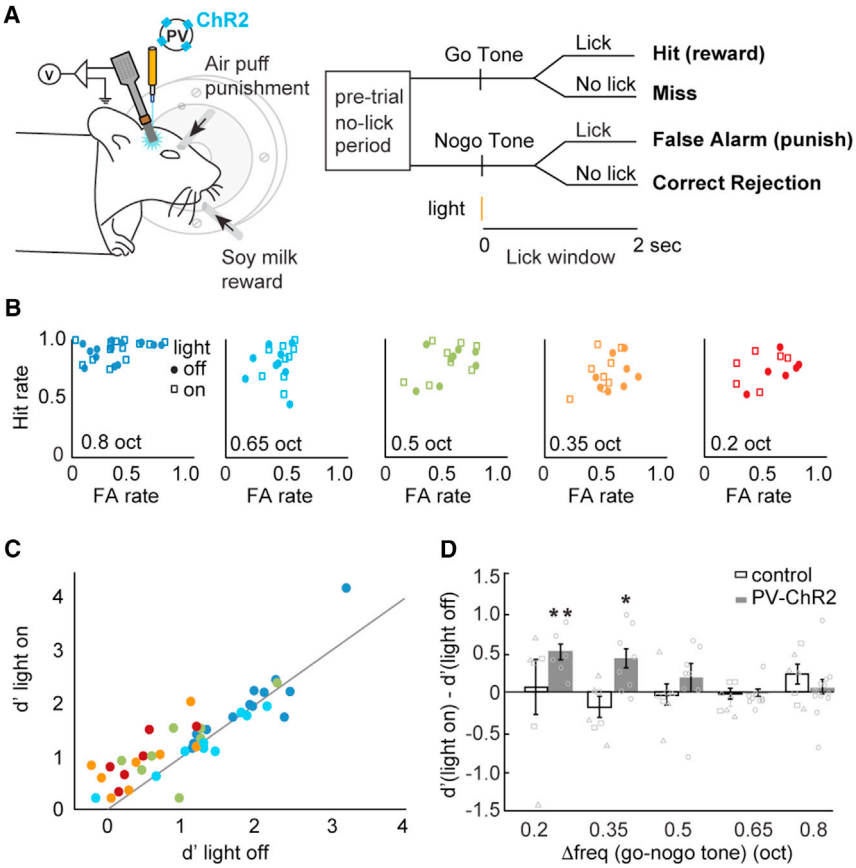

Figure 5. Tone Discrimination Improves with Light Excitation of A1 PV⁺ Interneurons

(A) Schematic of auditory go/no-go discrimination task with light stimulation.

(B) Hit rate versus FA rate in light-off (filled circles) and light-on (empty squares) conditions for each frequency difference between go and no-go trials in PV-ChR2 mice. Each pair of filled circle and empty square represents a single mouse tested at different frequency intervals.

(C) Discriminability index d′ without and with light for all frequency differences between go and no-go tones (n = 13, 9, 8, 8, 6 mice; color coded as in B).

(D) The d′ changes between light-off and light-on trials as a function of frequency interval between go and no-go tones for PV-ChR2 (**p = 0.008, *p = 0.021, paired t test) and control mice (Δ: wild-type control, n = 3, 4, 4, 4, 4 mice; □, PV-ChR2 before craniotomy control, n = 3, 3, 3, 3, 3 mice). Data show mean ± SEM.

See also Figure S6.

the medial geniculate body (MGB) and recorded activity in response to pure frequency tones as described earlier, with or without background WN (Figures 6A and 6B) or while performing light-induced activation of PV⁺ neurons in the auditory cortex (Figures 6H and 6I). In the MGB, background WN induced a slightly significant reduction in peak and baseline spike rates of responses to pure frequency tones (Figure 6C; $peak_{noWN}$ = 23.8 ± 2.6 Hz; $peak_{WN}$ = 21.5 ± 2.5 Hz; N_{mice} = 11; n_{su} = 122; p = 0.034; df = 121; LMM) (Figure 5D; $baseline_{noWN}$ = 9.8 ± 1.4 Hz; $baseline_{WN}$ = 8.5 ± 1.6 Hz; N_{mice} = 11; n_{su} = 122; p = 0.0094; df = 121; LMM). Plotting the mean of the peak aligned tuning curves showed a decrease in responses (Figures 6E and 6F; regression slope = 0.915; intersection = −1.05 Hz; r^2 = 0.936), corresponding to 13.0% suppression at peak and 7.9% suppression at baseline. We then estimated the frequency selectivity by computing the percentage of frequencies represented at a threshold of 0.5 of the peak spike rates. This showed a significant reduction in WN compared to no-WN trials (Figure 6G; $_{no\ WN}$ = 42.9% ± 3.3%; $_{WN}$ = 35.3% ± 3.5%; N_{mice} = 11; n_{su} = 122; p = 0.0013; df = 121; LMM). However, this increase in frequency selectivity could not be confirmed by a significant decrease of sigma in the small subset of cells whose tuning curves could be approximated by a Gaussian distribution (Figure S3C; n_{SU} = 7; p = 0.578; df = 6; LMM). In summary, the MGB activity was suppressed by WN both at peak and baseline. However, the overall effect of WN was less pronounced than in the cortex.

Next, we tested if cortical light-driven activation of PV⁺ neurons would similarly affect tone responses in the thalamus. We recorded activity in the MGB while performing cortical light-driven activation of PV⁺ neurons using similar light intensity levels described for the cortical recordings. We found a slightly significant decrease of peak and baseline spike rates (Figure 6J; $peak_{off}$ = 21.7 ± 2.5 Hz; $peak_{on}$ = 19.3 ± 2.2 Hz; N_{mice} = 7; n_{su} = 75; p = 0.0283; df = 74; LMM) (Figure 5K; $baseline_{off}$ = 9.7 ± 1.4 Hz; $baseline_{on}$ = 8.3 ± 1.1 Hz; N_{mice} = 7; n_{su} = 74; p = 0.0125; df = 74; LMM). The mean of peak aligned tuning curves exhibited a decrease in responses (Figures 6L and 6M; regression slope = 0.88; intersection = −0.19 Hz; r^2 = 0.897), corresponding to 12.7% suppression at peak and 6.1% suppression at baseline. We also quantified the percentage of frequencies represented as a function of a threshold normalized to peak spike rates. PV⁺ activation did not change the selectivity at a threshold of 0.5 of peak (Figure 6N; $_{Off}$ = 43.7% ± 3.3%; $_{On}$ = 41.6% ± 3.1%; N_{mice} = 7; n_{su} = 75; p = 0.2043; df = 74; LMM), as confirmed by the measurement of sigma of the Gaussian fits (Figure S3D; n_{SU} = 10; p = 0.105; df = 9; LMM). As for the cortical data, we verified that the preferred frequencies were not significantly shifted in either of the two perturbations (Figure S2B).

These recordings reveal that WN and cortical PV⁺ activation also modify tuning features in the thalamus. Since the thalamus is a relay station on the feedforward pathway to the cortex, it is not surprising that WN effects are observed here. In the case of cortical PV⁺ perturbations, corticothalamic projections probably echoed the cortical changes in thalamic circuits. PV⁺ perturbations, however, did not change the frequency selectivity of MGB neurons. In general, the effects of WN and light-driven activation of PV⁺ neurons were less pronounced in the thalamus as compared to the cortex.

We next developed a theoretical framework to investigate if thalamic or cortical changes in activity could explain the behavioral effects of WN and cortical light-induced PV^+ manipulation.

Modeling the Decoding of the Auditory Cortex Using a Simple Threshold Model Shows Improved Discriminability due to Suppression of Tuning Curves

Our results so far indicate a direct relationship between perturbations of cortical activity and behavioral outcome. But how can a suppression of cortical activity lead to an improvement in sensory discriminability? One possible explanation is that downstream circuits decode the sound-evoked activity in the primary auditory cortex in comparison to spontaneous activity levels. If only activity that exceeds a specific threshold is used for discrimination, a suppression of the tuning curves would mean that a narrower range of frequencies evokes activity that exceeds the threshold (Figure 7B). To explore this possible mechanism, we implemented a simplified model of a decoding circuit (Figure 7A) and used our experimentally measured mean tuning curves as input to the model.

The model assumes that frequency-tuned activity in A1 feeds into a layer of readout neurons in which a threshold is applied. Only activity that reaches the threshold evokes activity in the readout layer (Figure 7B). We assumed the activity in the readout neurons to follow Poisson variability, and we set up a decoder to classify between the go and no-go tones based on the single-trial activity in the readout layer (see STAR Methods). As a starting point, we used a threshold corresponding to 90% of the baseline spike rate in the control condition.

We simulated a model consisting of 800 readout neurons with preferred frequencies spanning eight octaves and computed the fraction of errors (error rate), as the frequency interval between go and no-go tones was varied (Figures 7C and 7E). The error rates generally increased as the frequency interval decreased, as expected, due to an increased similarity between the responses for go and no-go tones. While using the experimentally derived mean tuning curves for the control condition as a starting point, we then tried inducing a negative offset to the A1 activity (and hence in the input to the readout layer). An overall suppression in the A1 tuning curves led to a reduction in error rates, and this effect was most pronounced for small frequency intervals (Figure 7C). For values of negative offsets comparable to perturbed conditions (WN, PV^+ manipulation), we saw a clear improvement for frequency intervals smaller than 0.5 octaves (Figure 7C; colors indicate offset values for control, WN, and light-induced perturbations of PV^+ neurons).

To compare the performance of the decoder with the behavioral performance measured experimentally, we calculated the d' of the decoder by setting p(hit) = 1 − (error rate) and p(FA) = error rate and computed the difference in d' due to WN and light perturbations using experimentally derived tuning curves for control, WN, and light-induced PV^+ perturbations (Figures 7F and 7G; see STAR Methods for details). This revealed a clear improvement in d' for both WN and light perturbations for frequency intervals between go and no-go tones smaller than 0.5 octaves. We noted, however, that the decoder performed almost perfectly for larger frequency intervals, leaving little room for improvement at these intervals.

A key aspect of the model is the thresholding occurring in the layer of readout neurons, which causes a more frequency-selective activation in the perturbed conditions. To test the generality of this threshold assumption and the stability of our model results, we varied the threshold, expressed as spike count, over a wide range of values (Figures 7D and 7F). We computed the difference in decoding errors and the difference in d' for WN and light perturbations separately. This analysis showed that the improvements in decoding were not specific to the threshold values we used above, but occurred in a range of thresholds corresponding to approximately 50%–100% of the control baseline firing or to a spike count range between 0.30 and 0.60 spikes per trial. The experimentally recorded mean spontaneous spike count was 0.33 ± 0.46 SD across cortical neurons. If, however, no threshold was applied (corresponding to decoding the A1 activity directly), only a small improvement could be seen for the WN perturbation and no effect for light activation (as shown in Figures 7D and 7F with threshold, expressed in spike counts, set to zero).

Next, we investigated if the small changes observed in the MGB during WN or PV^+ perturbations would lead to a better discrimination in our model. Instead of using A1 activity as input to the readout layer, we used fits of the experimentally recorded MGB activity (Figure S7). We observed that the small changes during WN did give a better discrimination, though smaller than for A1 activity. However, the PV^+ perturbation did not give an increased discriminatory performance (Figure 7G), which confirms our conclusion that A1 activity seems to have a stronger weight than MGB activity in determining the discriminatory behavior.

Taken together, these results for our model illustrate a possible link between suppression in A1 activity and improvement in behavioral performance.

DISCUSSION

Our results demonstrate that tone discrimination is influenced by the tuning properties of primary auditory cortical neurons. We show that background WN suppresses responses to pure tones in cortical neurons. In an auditory go/no-go task, we find that background WN improves discrimination for pure frequency tones that are close together but does not affect performance for tones farther apart. Since WN selectively modifies tuning curves without significantly changing the fano factor or noise correlation, our data suggest that the brain might use neuronal tuning features to solve the discrimination task. Optogenetic manipulation of neurons in A1 selectively led to a similar suppression of A1 responses and behavioral effects as WN, even though the optical and WN manipulation were suggested to rely on different mechanisms (Figure 4). This supports the view that suppression of frequency tuning curves in the cortex led to the observed improvement in frequency discrimination. To gain insight into how activity in A1 neurons could relate to the discrimination of auditory stimuli and why background WN aids tone discrimination, we constructed a model of a simple decoding circuit and studied the discrimination performance in this model. The results of the model show that for neuronal parameters

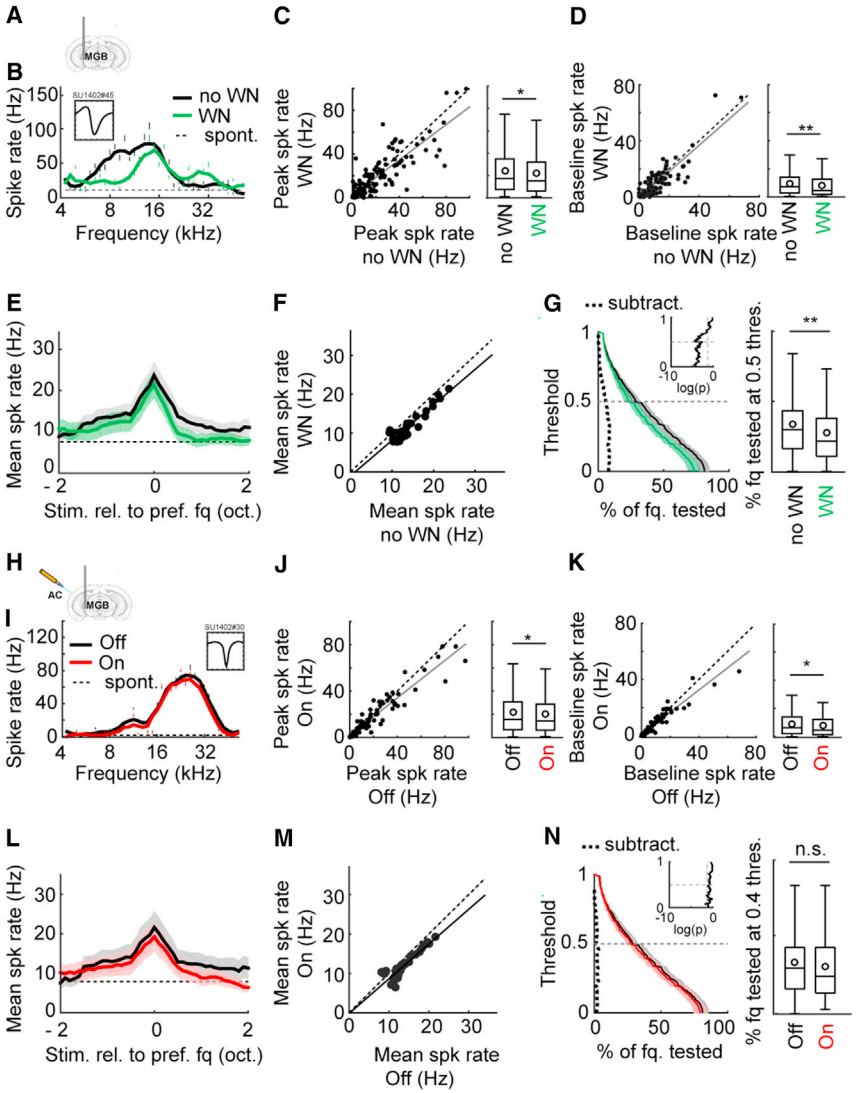

Figure 6. Thalamic Responses Weakly Reflect Cortical Tuning Changes during WN and Light-Induced Activation of Cortical PV$^+$ Neurons

(A) Schematics of extracellular recordings using a linear multi-electrode array through the MGB.

(B) Example of a SU's spike rates in response to pure tones in no-WN (black) or WN (green) background. All lines and symbols are as indicated in Figure 1.

(C and D) Scatterplot of peak (C) and baseline (D) spike rate in no-WN (black) versus WN (green) conditions (n_{su} = 122; N_{mice} = 11). Boxplots with peak spike rates (C, *p = 0.034, LMM) or baseline spike rates (D, **p = 0.0094, LMM). The dotted lines represent the unity lines.

(E) Mean of peak-aligned tuning curves. The dotted line represents spontaneous activity. Shaded areas indicate 5%-95% confidence intervals.

(F) Mean tuning curves from (E) plotted against each other (regression: slope = 0.915; intersection = −1.05 Hz; r^2 = 0.936).

(G) Percentage of frequencies represented as a function of a normalized spike rate threshold. The dotted line is the subtraction of no-WN (black) and WN (green) lines. Boxplots with percentage of frequency represented at a threshold of 0.5 of peak spike rate for no-WN and WN tuning curves (**p = 0.0013; df = 121; LMM). Inset shows p values comparing no WN and WN for frequencies represented at all thresholds of peak-normalized tuning curves using Wilcoxon test. The vertical dotted line shows p = 0.05.

(H) Schematics of extracellular recordings in the MGB combined with light-activation of PV-ChR2 cells in the A1.

(I) Expample of a SU's spike rates in response to pure tones in light-off (black) or light-on (red) conditions. All lines and symbols as indicated in Figure 1.

(J and K) Scatterplot of peak (J) and baseline (K) spike rate in light off (black) or light on (red) conditions (n_{su} = 75; N_{mice} = 7). Boxplots with peak spike rate (J, *p = 0.0283; LMM) or baseline spike rates (K, *p = 0.0125; LMM).

(L) Mean of peak-aligned tuning curves. The dotted line represents spontaneous activity. Shaded areas indicate 5%–95% confidence intervals.

(M) Mean tuning curves from (L) plotted against each other (regression: slope = 0.88; intersection = −0.19 Hz; r^2 = 0.897).

(N) Percentage of frequencies represented as a function of a normalized spike rate threshold. The dotted line is the subtraction of light-off (blakc) and light on (red) lines. Boxplots with percentage of frequencies represented at a threshold of 0.5 of peak spike rate for light-off and light-on tuning curves (p = 0.2043; LMM). Inset shows p values comparing light off and light on for frequencies represented at all thresholds of peak-normalized tuning curves using Wilcoxon test. The vertical dotted line shows p = 0.05. See also Figures S2 and S3.

matching our *in vivo* recordings in A1, and not in the MGB, the uncertainty of the sensory representation of go and no-go signals is reduced with the suppression of neuronal tuning curves only when the go and no-go signals are close to each other, in line with our behavioral observations. Together, our results suggest that the general tuning properties of A1 neurons directly shape discriminative performance and guide sensory-driven behavior.

Classical neural activity-to-behavior analysis (Britten et al., 1992; Yang et al., 2008; Znamenskiy and Zador, 2013) relies on a correlation between neurometric and psychometric functions to link neural activity and certain behaviors. However, to establish causality, the best available option is to perturb neurons while the animal engages in task-related behaviors (Panzeri et al., 2017). Ideally, perturbations should be subtle enough not to annihilate the neural activity or the behavior. By preserving neuronal activity during perturbations, we can look for activity features relevant toward the behavior. These features can be further implemented in models that may predict behavioral outcome. In our study, we used two different methods of perturbation to confirm causality—one natural, experienced on a daily basis by the auditory system (background WN), and one artificial (optogenetics)—to point to a particular feature of cortical activity. The results of these manipulations, producing similar cortical changes and similar improved behavioral outcomes, allow us to conclude that the response profile of A1

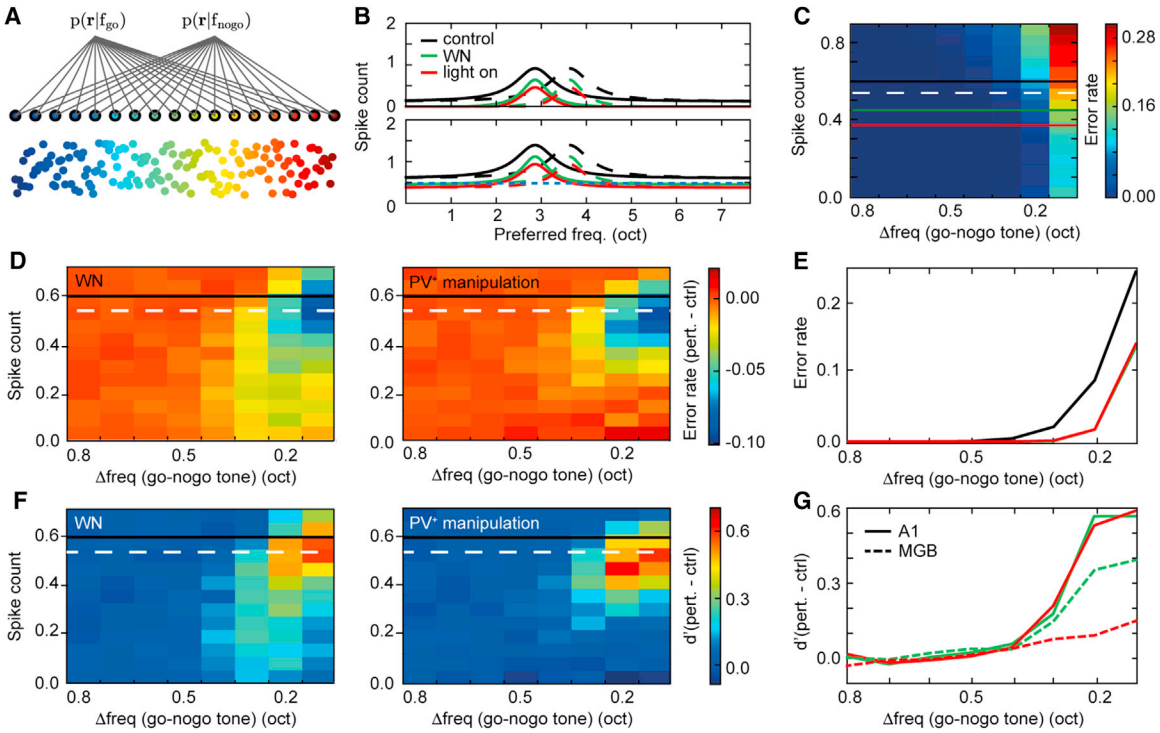

Figure 7. Modeling the Decoding of the Auditory Cortex Using a Simple Threshold Model Shows Improved Discriminability due to Suppression of Tuning Curves

(A) Illustration of model setup. A1 activity feeds to a layer of readout neurons where decoding occurs using a Bayes classifier.

(B) Bottom: Expected response in A1 for a go tone (solid lines) and a no-go tone (dashed lines) for the three different conditions indicated by color. The activity level that corresponds to the threshold in the readout layer is indicated by the dotted line. Top: Corresponding activity in the readout layer.

(C) Error rate for control tuning curve shifted to different baseline level (y scale). Solid lines indicate baseline levels for control (black), WN (green), and PV^+ activation (red). Dashed white line indicates the default threshold set at 90% of control baseline.

(D) Difference in error rate compared to control for WN (left) and PV^+ activation (right) as a function of the threshold level in the readout layer (y scale). Solid black lines indicate control baseline, and dashed white line indicates default threshold.

(E) Error rate for default threshold in the three different conditions.

(F) Difference in d′ compared to control for WN (left) and PV^+ activation (right) as a function of the threshold level in the readout layer (y scale). Solid black lines indicate control baseline, and dashed white lines indicate default threshold.

(G) Difference in d′ for default threshold compared with control for WN (green) and PV^+ activation (red).

See also Figure S7.

neurons is not only correlated, but also directly involved in shaping the formation of tone percepts.

In our experiments, continuous WN did not show any increase in mean excitatory activity, as compared to silence (Figure 1B). This is counterintuitive—in our ears, continuous WN can be perceived—but not new (Liang et al., 2014; Teschner et al., 2016) or surprising. Indeed, the mean A1 excitatory response to constant sounds, even as short as 100 ms, is mainly observed at the tone onset and sometimes at the tone offset, but not during the tone (Shiramatsu et al., 2016). We cannot, however, rule out whether individual A1 neurons, or neurons outside of A1, respond strongly to continuous WN. Adaptation to continuous WN has been shown to increase as one ascends the auditory pathway (Rabinowitz et al., 2013).

The mechanisms leading to the suppression of cortical tuning curves by background WN are also still unresolved. Our experiments indicate that background WN modifies auditory responses subcortically already (Figures 6A–6G) and that the activation of cortical PV^+ neurons might not be the main driver behind this suppression (Figure 4). We cannot rule out that other interneurons in the cortex, or PV^+ neurons activated at different timing than the ones imposed by optogenetics, might emphasize the suppression already observed in the thalamus. It has indeed been shown that two tones presented simultaneously sharpen tuning curves via lateral inhibition throughout the auditory pathway (Kato et al., 2017; Shamma and Symmes, 1985). Whether a similar mechanism might be involved when a tone is played simultaneously with WN is not known. Further work would be needed to disentangle the mechanisms behind the effects of background WN on tone responses.

We used the optogenetic approach targeted at inhibitory neurons to ask whether the cortical effects of the background WN were enough to explain the discrimination performance, and we hence affected neurons in A1 directly. Previous work has already shown that PV^+ neuron activation suppresses

tuned responses and improves sensory acuity. A study in the auditory cortex finds that PV^+ neuron activation causes improved perceptual discrimination between a phasic and a continuous pure frequency tone in a prepulse inhibition behavioral paradigm (Aizenberg et al., 2015). With the same paradigm, it has also been shown that PV^+ manipulation improves or impairs behavioral performance due to modifications in frequency tuning (Briguglio et al., 2018). Here, it is argued that an increased signal-to-noise ratio in A1 responses is the underlying mechanism for the improved performance. In our study, we rather see a decrease in the signal-to-noise ratio, measured as the peak-to-baseline ratio. Since the behavioral paradigms are different in both studies—the prepulse inhibition test relying on a startle response and the go/no-go test based on a decision of the mouse to react to a sound—it is difficult to compare both studies.

PV^+ perturbation might lead to changes in other features of the cortical activity than those analyzed here. Interneurons, for example, have been shown to play an important role in increasing temporal precision and reducing the randomness of the cortical operation (Wehr and Zador, 2003; Moore and Wehr, 2013) or in enabling context-dependent behavior (Kuchibhotla et al., 2017). Activating PV^+ interneurons could also decrease intracortical activity and promote activity locked to a strong thalamic drive (Krause et al., 2019). In addition, PV^+ activation has been shown to enhance functional connectivity in columnar cortical circuits (Hamilton et al., 2013). Our data cannot tell whether such mechanisms are at play with the perturbations explored here.

The results from both WN and light-driven PV^+ activation show that discrimination performance improves only for small frequency intervals, while large intervals remain unaffected. This suggests that the perturbation effects are specific in manipulating particular constraints determined by the encoding of pure tones across a population of A1 neurons and not because of changes in a global parameter such as attention or motivation. However, our analysis cannot rule out whether specific changes in individual or subgroups of cells could be responsible for the increase in discriminability. Both perturbations induce heterogeneous changes to individual cells (Figures 1D, 1E, 3B, and 3C). The fact that the mean activity of the neuronal population correlates with behavioral performance suggests that the brain integrates activity across a larger population.

One could speculate whether the fact that the learning phase of the behavioral paradigm was done without background WN and without light stimulation could have any perceptual learning consequences that could influence the results of the testing phase. However, if this were the case, we would expect a bigger effect at the no-go frequency used during the learning phase (i.e., 0.8 oct) and not at frequencies the mice had not been exposed to during the learning phase (>0.8 oct), or at least the same effect on all frequencies tested. This was not reflected in our results.

Finally, although the two perturbations allow us to identify cortical tuning curves to shape tone discrimination performance, A1 would not be expected to be the sole contributor to the integrated auditory information relevant for solving the behavioral task.

A basic function of the sensory system is to extract relevant information from a more-or-less distracting background noise. We demonstrate that cortical representation of pure tones adapts during noise by suppressing pure tone responses and thereby increasing selectivity at the expense of the mean amplitude of the spike response. As a consequence, the mice can more easily distinguish tones within a narrow frequency band. So why would auditory acuity improve during noise? It is possible that total silence is an unnatural context and that the brain is simply optimized for more noisy environments. Alternatively, the brain could promote discrimination at the expense of precision in other sound features, such as loudness, in the competing demands of discrimination versus detection (Guo et al., 2017). Future work will be required to determine how the many effects of WN already described at the perceptual level (Kishon-Rabin et al., 2008; Zeng et al., 2000) are reflected in the cortical neuronal activity.

STAR★METHODS

Detailed methods are provided in the online version of this paper and include the following:

- KEY RESOURCES TABLE
- LEAD CONTACT AND MATERIALS AVAILABILITY
- EXPERIMENTAL MODEL AND SUBJECT DETAILS
- METHOD DETAILS
  - Surgical procedure
  - Auditory stimulation
  - Extracellular recordings
  - Behavioral experiments
  - Optogenetics
  - Intracellular and cell-attached recordings
  - Immunohistochemistry
  - Population model
- QUANTIFICATION AND STATISTICAL ANALYSIS
  - Data processing
  - Data analysis
  - Statistics
- DATA AND CODE AVAILABILITY

SUPPLEMENTAL INFORMATION

Supplemental Information can be found online at https://doi.org/10.1016/j.celrep.2019.10.049.

ACKNOWLEDGMENTS

This work was supported by grants from the Lundbeck Foundation (fellowship to T.R.B.) and the Swiss National Science Foundation (ERC Transfer grant to T.R.B.).

AUTHOR CONTRIBUTIONS

Conceptualization, R.K.C., H.L., M.N., and T.R.B.; Methodology, R.K.C., H.L., and T.R.B.; Investigation, R.K.C., M.N., and T.R.B.; Writing - Review & Editing, R.K.C., H.L., M.N., and T.R.B.; Funding Acquisition, T.R.B.; Supervision, T.R.B.

DECLARATION OF INTERESTS

The authors declare no competing interests.

Received: August 24, 2018
Revised: July 25, 2019
Accepted: October 9, 2019
Published: November 12, 2019

REFERENCES

Aizenberg, M., Mwilambwe-Tshilobo, L., Briguglio, J.J., Natan, R.G., and Geffen, M.N. (2015). Bidirectional Regulation of Innate and Learned Behaviors That Rely on Frequency Discrimination by Cortical Inhibitory Neurons. PLoS Biol. *13*, e1002308.

Alain, C., Quan, J., McDonald, K., and Van Roon, P. (2009). Noise-induced increase in human auditory evoked neuromagnetic fields. Eur. J. Neurosci. *30*, 132–142.

Atiani, S., Elhilali, M., David, S.V., Fritz, J.B., and Shamma, S.A. (2009). Task difficulty and performance induce diverse adaptive patterns in gain and shape of primary auditory cortical receptive fields. Neuron *61*, 467–480.

Bathellier, B., Ushakova, L., and Rumpel, S. (2012). Discrete neocortical dynamics predict behavioral categorization of sounds. Neuron *76*, 435–449.

Briguglio, J.J., Aizenberg, M., Balasubramanian, V., and Geffen, M.N. (2018). Cortical Neural Activity Predicts Sensory Acuity Under Optogenetic Manipulation. J. Neurosci. *38*, 2094–2105.

Britten, K.H., Shadlen, M.N., Newsome, W.T., and Movshon, J.A. (1992). The analysis of visual motion: a comparison of neuronal and psychophysical performance. J. Neurosci. *12*, 4745–4765.

Brugge, J.F., Reale, R.A., and Hind, J.E. (1998). Spatial receptive fields of primary auditory cortical neurons in quiet and in the presence of continuous background noise. J. Neurophysiol. *80*, 2417–2432.

Carcea, I., Insanally, M.N., and Froemke, R.C. (2017). Dynamics of auditory cortical activity during behavioural engagement and auditory perception. Nat. Commun. *8*, 14412.

Centanni, T.M., Sloan, A.M., Reed, A.C., Engineer, C.T., Rennaker, R.L., II, and Kilgard, M.P. (2014). Detection and identification of speech sounds using cortical activity patterns. Neuroscience *258*, 292–306.

Ehret, G., and Schreiner, C.E. (2000). Regional variations of noise-induced changes in operating range in cat AI. Hear. Res. *141*, 107–116.

Evans, E.F., Ross, H.F., and Whitfield, I.C. (1965). The spatial distribution of unit characteristic frequency in the primary auditory cortex of the cat. J. Physiol. *179*, 238–247.

Francis, N.A., Winkowski, D.E., Sheikhattar, A., Armengol, K., Babadi, B., and Kanold, P.O. (2018). Small Networks Encode Decision-Making in Primary Auditory Cortex. Neuron *97*, 885–897.e6.

Fritz, J., Shamma, S., Elhilali, M., and Klein, D. (2003). Rapid task-related plasticity of spectrotemporal receptive fields in primary auditory cortex. Nat. Neurosci. *6*, 1216–1223.

Goldstein, M.H., Jr., Abeles, M., Daly, R.L., and McIntosh, J. (1970). Functional architecture in cat primary auditory cortex: tonotopic organization. J. Neurophysiol. *33*, 188–197.

Guo, W., Chambers, A.R., Darrow, K.N., Hancock, K.E., Shinn-Cunningham, B.G., and Polley, D.B. (2012). Robustness of cortical topography across fields, laminae, anesthetic states, and neurophysiological signal types. J. Neurosci. *32*, 9159–9172.

Guo, W., Clause, A.R., Barth-Maron, A., and Polley, D.B. (2017). A Corticothalamic Circuit for Dynamic Switching between Feature Detection and Discrimination. Neuron *95*, 180–194.e5.

Hackett, T.A., Barkat, T.R., O'Brien, B.M., Hensch, T.K., and Polley, D.B. (2011). Linking topography to tonotopy in the mouse auditory thalamocortical circuit. J. Neurosci. *31*, 2983–2995.

Hamilton, L.S., Sohl-Dickstein, J., Huth, A.G., Carels, V.M., Deisseroth, K., and Bao, S. (2013). Optogenetic activation of an inhibitory network enhances feedforward functional connectivity in auditory cortex. Neuron *80*, 1066–1076.

Henning, G.B. (1967). Frequency discrimination in noise. J. Acoust. Soc. Am. *41*, 774–777.

Javel, E.R., Jesteadt, W.H., and Bilger, C. (1971). Frequency discrimination in noise. J. Acoust. Soc. Am. *41*, 774–777.

Kato, H.K., Asinof, S.K., and Isaacson, J.S. (2017). Network-Level Control of Frequency Tuning in Auditory Cortex. Neuron *95*, 412–423.e4.

Kishon-Rabin, L., Gam, S., Shiff, T., Rembrand, R., and Roth, D.A. (2008). Speech perception enhanced by noise in listeners with normal hearing. J. Basic Clin. Physiol. Pharmacol. *19*, 237–248.

Klampfl, S., David, S.V., Yin, P., Shamma, S.A., and Maass, W. (2012). A quantitative analysis of information about past and present stimuli encoded by spikes of A1 neurons. J. Neurophysiol. *108*, 1366–1380.

Krause, B.M., Murphy, C.A., Uhlrich, D.J., and Banks, M.I. (2019). PV+ Cells Enhance Temporal Population Codes but not Stimulus-Related Timing in Auditory Cortex. Cereb. Cortex *29*, 627–647.

Kuchibhotla, K.V., Gill, J.V., Lindsay, G.W., Papadoyannis, E.S., Field, R.E., Sten, T.A., Miller, K.D., and Froemke, R.C. (2017). Parallel processing by cortical inhibition enables context-dependent behavior. Nat. Neurosci. *20*, 62–71.

Labiak, J.M., and Wilson, W.R. (1974). Effect of contralateral broad-band noise on frequency discrimination. Acta Otolaryngol. *77*, 29–36.

Liang, F., Bai, L., Tao, H.W., Zhang, L.I., and Xiao, Z. (2014). Thresholding of auditory cortical representation by background noise. Front. Neural Circuits *8*, 133.

Lin, I.C., Okun, M., Carandini, M., and Harris, K.D. (2015). The Nature of Shared Cortical Variability. Neuron *87*, 644–656.

Martin, B.A., Sigal, A., Kurtzberg, D., and Stapells, D.R. (1997). The effects of decreased audibility produced by high-pass noise masking on cortical event-related potentials to speech sounds/ba/and/da. J. Acoust. Soc. Am. *101*, 1585–1599.

Mesgarani, N., David, S.V., Fritz, J.B., and Shamma, S.A. (2009). Influence of context and behavior on stimulus reconstruction from neural activity in primary auditory cortex. J. Neurophysiol. *102*, 3329–3339.

Moore, A.K., and Wehr, M. (2013). Parvalbumin-expressing inhibitory interneurons in auditory cortex are well-tuned for frequency. J. Neurosci. *33*, 13713–13723.

Panzeri, S., Harvey, C.D., Piasini, E., Latham, P.E., and Fellin, T. (2017). Cracking the Neural Code for Sensory Perception by Combining Statistics, Intervention, and Behavior. Neuron *93*, 491–507.

Phillips, D.P. (1990). Neural representation of sound amplitude in the auditory cortex: effects of noise masking. Behav. Brain Res. *37*, 197–214.

Rabinowitz, N.C., Willmore, B.D., King, A.J., and Schnupp, J.W. (2013). Constructing noise-invariant representations of sound in the auditory pathway. PLoS Biol. *11*, e1001710.

Reig, R., Zerlaut, Y., Vergara, R., Destexhe, A., and Sanchez-Vives, M.V. (2015). Gain modulation of synaptic inputs by network state in auditory cortex in vivo. J. Neurosci. *35*, 2689–2702.

Seriès, P., Latham, P.E., and Pouget, A. (2004). Tuning curve sharpening for orientation selectivity: coding efficiency and the impact of correlations. Nat. Neurosci. *7*, 1129–1135.

Seybold, B.A., Phillips, E.A.K., Schreiner, C.E., and Hasenstaub, A.R. (2015). Inhibitory Actions Unified by Network Integration. Neuron *87*, 1181–1192.

Shamma, S.A., and Symmes, D. (1985). Patterns of inhibition in auditory cortical cells in awake squirrel monkeys. Hear. Res. *19*, 1–13.

Shiramatsu, T.I., Noda, T., Akutsu, K., and Takahashi, H. (2016). Tonotopic and Field-Specific Representation of Long-Lasting Sustained Activity in Rat Auditory Cortex. Front. Neural Circuits *10*, 59.

Sollini, J., Alves-Pinto, A., and Sumner, C.J. (2016). Relating approach-to-target and detection tasks in animal psychoacoustics. Behav. Neurosci. *130*, 393–405.

Teschner, M.J., Seybold, B.A., Malone, B.J., Hüning, J., and Schreiner, C.E. (2016). Effects of Signal-to-Noise Ratio on Auditory Cortical Frequency Processing. J. Neurosci. *36*, 2743–2756.

Von Bekesy, G. (1960). Experiments in Hearing (McGraw-Hill Book Company).

Wehr, M., and Zador, A.M. (2003). Balanced inhibition underlies tuning and sharpens spike timing in auditory cortex. Nature *426*, 442–446.

Whiting, K.A., Martin, B.A., and Stapells, D.R. (1998). The effects of broadband noise masking on cortical event-related potentials to speech sounds /ba/ and /da/. Ear Hear. *19*, 218–231.

Yang, Y., DeWeese, M.R., Otazu, G.H., and Zador, A.M. (2008). Millisecond-scale differences in neural activity in auditory cortex can drive decisions. Nat. Neurosci. *11*, 1262–1263.

Zeng, F.G., Fu, Q.J., and Morse, R. (2000). Human hearing enhanced by noise. Brain Res. *869*, 251–255.

Zhou, Y., and Wang, X. (2010). Cortical processing of dynamic sound envelope transitions. J. Neurosci. *30*, 16741–16754.

Znamenskiy, P., and Zador, A.M. (2013). Corticostriatal neurons in auditory cortex drive decisions during auditory discrimination. Nature *497*, 482–485.

STAR★METHODS

KEY RESOURCES TABLE

REAGENT or RESOURCE	SOURCE	IDENTIFIER
Antibodies		
Rabbit anti-PV	Swant	Cat # PV25; RRID: AB_2631173
Donkey anti rabbit Alexa-594	Thermo Fisher Scientific	Cat # R37119; RRID: AB_2556547
DAPI antibody	Thermo Fisher Scientific	Cat # D1306; RRID: AB_2629482
Experimental Models: Organisms/Strains		
Mice: C57BL6/6J	Janvier	N/A
Mice: PV-Cre knockin line	Jackson	Cat # 017320
Mice: Ai32 line	Jackson	Cat # 024109
Software and Algorithms		
Klusta-Suite	Cortical Processing Laboratory (UCL)	https://github.com/klusta-team/
MATLAB	Mathworks	https://www.mathworks.com/
Python	Python Software Foundation	Python 2.7
Other		
Silicon Probes (A4x8, A1x32)	Neuronexus	A4x8-5mm-50-200-177
Silicon Probes (A4x8, A1x32)	Neuronexus	A1x32-5mm-25-177

LEAD CONTACT AND MATERIALS AVAILABILITY

Further information and requests for resources and reagents should be directed to and will be fulfilled by the Lead Contact, Tania Rinaldi Barkat (tania.barkat@unibas.ch). This study did not generate any new or unique reagents.

EXPERIMENTAL MODEL AND SUBJECT DETAILS

All experimental procedures were carried out according to the Basel University, Switzerland and Copenhagen University, Denmark, animal care and use committee guidelines. To target the opsins to PV^+ interneurons, we used PV-Cre knock-in line with C57BL/6J background (JAX stock number 017320, Jackson Laboratories, ME, USA). This strain drives expression of Cre in PV^+ interneurons of the cortex with minimal leak. We crossed this line to the Ai32 line (JAX stock number 024109 with C57BL/6 background), which encodes the light-gated depolarizing cation channel channelrhodopsin-2 conjugated to e-YFP after a floxed stop cassette under the CAG promoter. Wild-types were C57BL/6J mice (Janvier, France). For all experiments, we used adult (7 to 12 weeks old) male or female mice without distinction. Unless the mice were food-deprived (Figures 2 and 5), they were housed in groups of 2 to 5 under a 12hr/12hr light/dark cycle, and allowed to get food and water ad libido.

METHOD DETAILS

Surgical procedure

During surgery, mice were anesthetized with isoflurane (4% for induction, 1.5 to 2.5% for maintenance), and their bodies maintained at 37°C for the duration of the surgery with a heating pad (FHC, ME, USA). A custom-made stainless-steel head-restraint post was fixed on the bone on top of the left hemisphere, and used to head-fix the animals. Using a scalpel, a craniotomy (~2x2 mm^2) was performed just above the auditory cortex. The dura was left intact and was covered with silicone oil and a silicone casting compound (Kwik cast, World Precision Instruments, Inc. FL, USA)) to protect the brain during the recovering period from the anesthesia. The animals were allowed to recover from anesthesia in their homecage for at least one hour.

Auditory stimulation

Sounds were generated with a complex auditory processor (RZ6, Tucker Davis Technologies, FL, USA) at 200 kHz sampling rate and played through an MF1 speaker (Tucker Davis Technologies. FL, USA) positioned at 5 cm from the mouse's left ear. Pure tones (50 ms duration, 4 ms cosine on/off ramps) from 4 to 48.5 kHz in 0.1 octave increments were played with randomized inter-tone intervals of 500 to 1000 ms at 60 dB SPL and repeated 10 times (Figures 1 and 3). For the WN experiments (Figures 1 and 2), a continuous WN of

50 dB SPL (bandwidth of 1 to 64kHz) was played in addition to the tones, through the same MF1 speaker. For the behavioral experiments, similar pure tones of the go and no-go tone frequencies were played at 60 (Figure 2) or 80 dB SPL (Figure 5). Stimuli were calibrated with a wide-band ultrasonic acoustic sensor (Model 378C01, PCB Piezotronics, NY, USA).

Extracellular recordings

After recovery from the surgery, mice were placed in a cardboard tube (4 cm diameter) and the head-post was attached to a holder fixed to the soundbox. The mice could move their body inside the tube while the head was fixed. The silicone cast was then gently removed and a 4x8 electrode (A4x8-5mm-50-200-177-A32, Neuronexus, MI, USA) was inserted in A1 orthogonal to the brain surface (as confirmed through postmortem electrode track reconstructions in a subset of cases; Figure S5B) with a motorized stereotaxic micromanipulator (DMA-1511, Narishige, Japan) at a constant depth (tip of electrode at 625 ± 25 μm from pia). Recording sites spanned 600 μm in the caudal-rostral axis and 350 μm in depth traversing the granular layer including sites in the supra -and sub granular layer. Recordings from the primary auditory cortex were confirmed in each animal by the increase in preferred frequency from the most caudal to the most rostral shaft of the 4-shaft electrodes, confirming the tonotopic organization typical of A1.

For the thalamic recordings, the craniotomy was bigger in the direction of the midline in order to allow a vertical access to the MGB. These recordings were performed with a 1x32 electrode ((A1x32-5mm-25-177-A32, Neuronexus, MI, USA) inserted vertically at about 0.2 mm anterior to lambda and 0.8 mm lateral to the midline, to a depth of about 3mm and spanning 800 μm, targeting the ventral part of the MGB. No post hoc staining was performed to confirm the locations of the recording electrodes as a function of the MGB subdivisions.

Behavioral experiments

Mice were implanted with a metal head-restraint post at 7-9 weeks after birth under isoflurane anesthesia. After recovery from the surgery for a couple of days, mice were food restricted. They were then adapted to the head restrain and taught to associate a sound with a reward availability. During subsequent training, they were trained to differentiate two pure tones of different frequencies (typically 7 kHz for the go tone, and 12 kHz for the no-go tone). If the mice licked as a response to a go tone in the reward time window (typically 2 s), they received a drop of soy milk as reward and the trial was considered a hit. If they did not lick in the reward window, it was considered a miss trial. If the mice did not lick as a response to a no-go tone in the reward window, it was considered a correct rejection (CR), which was not rewarded. If they licked to a no-go tone, it was considered a false alarm trial (FA), and the mice received a mild air puff oriented toward the right eye, and a time out (3 s) until the next trial could start (Figures 2A and 5A). Sounds were delivered without preceding cues at random interstimulus intervals ranging from 3 to 5 s. If the mice licked in this interstimulus interval, the trial was aborted. Licks were detected with a piezo film attached to the reward spout. All experiments were performed in a sound proof box (IAC acoustics, Hvidovre, Denmark) and monitored from outside the soundbox with a camera (C920, Logitech, Switzerland). Behavioral control and data collection were carried out with custom-written programs using a complex auditory processor (RZ6, Tucker Davis Technology, FL, USA), and further analyzed with MATLAB (MathWorks, MA, USA). Once the mice achieved a consistent discriminability ($d' > 2$), they were considered well trained and moved on to the discrimination test, where the no-go tone progressively got closer to the go tone for each additional session (no-go tone tested: 12, 11, 10, 9, 8 kHz), until the mice were not able to discriminate both tones anymore, or until they did not want to perform anymore (Figures S4D and S4E). Not all mice were tested at all five frequency intervals. In this discrimination test, each session typically lasted about 10 minutes (presentation of about 50 go tones and 50 no-go tones). All sessions with a hit rate below 50%, where mice were not motivated or satiated, were eliminated. For the experiments with the WN, the same tests were done but the mice were exposed to a continuous WN sound in addition to the go and no-go pure frequency tones. The sessions with no WN and with WN were following each other for each No-go tone (Figure S4B). In order to make sure that the observed effects were not due to the order of presentation of the WN or no WN sessions, the order of no WN and WN was mixed in the different testing days, so that some days the WN was played before the no WN conditions, and some days the no WN was played before the WN conditions. All sessions of the testing phase were then averaged for each WN and no WN conditions and each No-Go tone per animal. For the experiments with optogenetics, the same tests were done but a laser light on top of A1 was turned on during the tone duration every second trial. WN and optogenetics were not applied during behavioral training.

Optogenetics

Once the electrodes were inserted, the cortical surface just above the electrodes was illuminated with light through a 50 μm diameter fiber optic connected to a 473 nm laser (BL473T3-100FC, Shanghai Laser & Optics Century Co, Shanghai, China) on every second trial. The light illumination lasted 50 ms and started at tone onset. Laser power was determined so that recording with blue light suppressed firing to about 50% of light-off condition, on average (Figures S5C, S5D, S6A, and S6B).

Intracellular and cell-attached recordings

Mice were kept on isoflurane anesthesia (1%–1.4%) for these recordings. Whole-cell and cell-attached recordings were made with an Axopatch 700B amplifier (Molecular Devices, CA, USA). Patch pipettes (4-7 MOhm) were filled with an intracellular solution containing (in mM) 135 K-gluconate, 4 KCl, 10 Na phosphocreatine, 10 HEPES, 4 MgATP, 0.3 Na_3GTP, pH adjusted to 7.3 with KOH, Biocytin 2 mg/ml. Recordings were made under voltage-clamp mode for cell-attached recordings and current-clamp mode

for whole-cell recordings. The light effect was tested in a 1.0 s off - 0.5 s on cycle. Mean number of spikes or time spent in the up-state relative to the down-state from 20-50 cycles where used to compute the level of suppression for cell-attached and whole-cell modes, respectively.

Immunohistochemistry

To confirm the specific expression of genetically encoded ChR2 in PV^+ interneurons, we performed PV immunohistochemistry (Figure S5A). Mice were transcardially perfused with 4% PFA under deep anesthesia. Brains were extracted from the skull and post-fixed in 4% PFA for 24 hours at 4°C, then washed in PBS and sliced coronally at 100 μm thickness on a vibratome. Fixed brain sections were incubated for 2 h at room temperature in blocking buffer containing PBS with 0.5% v/v Triton X-100 (Sigma-Aldrich, Switzerland) and 5% Donkey serum (Bio-Rad, UK). The buffer solution was removed and the slices were incubated at 4°C for 4 days in the primary antibody (rabbit anti-PV, 1:500, Swant, Switzerland). Slices were then washed and incubated at room temperature for 2 hours in the secondary antibody (Donkey anti rabbit Alexa-594, 1:500, Invitrogen, CA, USA). Slices were then washed and incubated at room temperature for 15 minutes with a DAPI solution (Molecular Probes, USA), washed, mounted and coverslipped using Fluoromount (Sigma-Aldrich, Switzerland). Images were acquired with a 20x objective on a confocal microscope (LSM 710, Carl Zeiss Inc, Switzerland).

Population model

We considered a population of readout neurons that receive frequency tuned input from A1. The population consisted of 800 neurons with preferred frequencies distributed over 8 octaves, in steps of 0.01 octaves. The activity of each neuron was set by f(I) = I-threshold, for I > threshold, and 0 otherwise. The input I to each neuron was given by a fit to the experimentally measured mean tuning curves using the following lorentzian function:

$$I(f) = r_{baseline} + (r_{peak} - r_{baseline}) \frac{0.5w^2}{(f - f_{bf})^2 + 0.5w^2}$$

where $r_{baseline}$ and r_{peak} corresponds to baseline and peak firing rate, w denotes the width of the tuning curve and f_{bf} is the best frequency of each neuron. We considered the activity within a 50 ms window and used the spike count within this window to denote activity levels. The output of each neuron in each trial was simulated by drawing a random number from a Poisson distribution with the intensity given by f(I) described above.

To decode the activity in the layer of readout neurons we used a Bayes classifier to determine which of the two tone frequencies (f_{go}, f_{nogo}) was most likely to have generated the spike response $\boldsymbol{r}$:

$$\hat{f} = \underset{f}{\operatorname{argmax}} \log p(\boldsymbol{r}|f)p(f)$$

with $f \in \{f_{go}, f_{nogo}\}$ and $p(f_{go}) = p(f_{nogo}) = 1/2$. Throughout this study we generated activity corresponding to a go tone and used to decoder to discriminate the go tone from a no-go tone with varying frequency intervals between go and no-go tone.

The activity in the readout layer was assumed to be generated by independent Poisson processes for each neuron and we calculated the log likelihood of a specific spike count response across the population using the Poisson distribution:

$$\log p(\boldsymbol{r}\,|\,f) = \sum_{i=1}^{n} \log p(r_i\,|\,f) = \sum_{i=1}^{n} \log \frac{e^{-\mu_i(f)} \mu_i(f)^{r_i}}{r_i!}$$

For each simulation of an error rate we generated 10000 trials of go tone activity and computed the error rate as the fraction of incorrect classifications. To compute the discriminability index d' we calculated hit and false alarm rates as p(hit) = 1-(error rate) and p(fa) = error rate, respectively. To account for variability unrelated to sensory evidence and to avoid unrealistically high d' values we introduced additional errors in 10% of the trials (thereby setting the minimum error rate to 0.1) in the d' simulations.

The model implementation was done in Python 2.7 using packages numpy, scipy and matplotlib (Python Software Foundation).

QUANTIFICATION AND STATISTICAL ANALYSIS

Data processing

Responses from extracellular recordings were digitized with a 32-channel recording system (RZ5 Bioamp processor, Tucker Davis Technologies, FL, USA) at 24'414Hz. Single units (SUs) were identified from raw voltage traces using a semi-automated spike-detection and clustering algorithm followed by a manual clustering according to their interspike interval distributions, waveform consistency and presence in neighboring recording sites with Klusta-Suite (Klusta, open source software) and further analyzed with custom software in MATLAB (Mathworks, MA, USA). For intracellular recordings, data were filtered at 2 kHz, sampled at 10 kHz and digitized by Digidata 1440 (Molecular Devices, CA, USA), and analyzed with custom software in MATLAB (Mathworks, MA, USA).

Data analysis

Raw tuning curves were smoothed using a 3-point mean filter. The raw data was smoothed to reduce noise and emphasize the typical bandwidth selective shape of tuning curves. The smoothed data was only used when representing tuning of single SU examples and during the calculation of preferred frequency. Raw tuning curves were used for calculation of all other analysis parameters.

For Figure S3, tuning curves of SU were analyzed by fitting a Gaussian function to the mean spike rates (10 trials per frequency, 50 ms time window) during pure tone stimulation. Only response profiles with a certain precision of the fit ($r^2 > 0.5$) were included in the analysis. The sigma of the Gaussian curve (σ) was taken as a measure of frequency selectivity (2 x σ cover the frequency range containing 68.27% of the evoked spikes, and therefore directly relates to tuning width).

Statistics

For electrophysiology, all statistical values were reported as means ± standard error (SEM) and plotted as boxplots including mean (circle) and median, 25^{th}-75^{th} and 10^{th}-90^{th} percentiles (box), with n representing the number of SUs or pairs of SUs and N representing the number of animals. Degrees of freedom (df) is given as number of observations – 1. We used a linear mixed model (LMM) analysis of variance to compare differences between no WN and WN trials or light off and light on trials, with WN or light conditions as fixed effects and individual mouse number, cluster numbers and shank number as random effects. For the p values of the insets in Figures 1H, 3F, 6G, and 6N, the Wilcoxon test was used because we did it over a large dataset (for threshold values of 0 to 1 in 0.01 steps) where using LMM is not practical. We further confirmed that the LMM and Wilcoxon tests yielded p values in the same range, as illustrated by the p values comparing % frequencies tested at 0.5 threshold across conditions computed with LMM (bloxplot, right panels) or Wilcoxon (inset, left panels) respectively: 0.004 and 0.0011 (Figure 1H), 0.0011 and 0.0032 (Figure 3F), 0.0013 and 0.0017 (Figure 6G), 0.2043 and 0.265 (Figure 6N). For the LMM, statistical tests were carried out in R version 0.99.896 using the relevant packages lme4 and LMERConvenienceFunctions. p values were computed from the initial LMM model using the pamer.fnc function as part of the package LMERConvenienceFunctions. Pamer.fnc performs an ANOVA based on the lmer model. For behavioral experiments, all statistical values were reported and plotted as mean ± SEM, with N representing the number of animals. Statistical testing was carried out in Microsoft Excel using Student's two-tailed paired t test. The reason to use LMM for physiology is to take into account statistical dependencies due to random effects such as single units acquired from the same animal or units in close proximity recorded from the same electrode shank. For the behavioral data however, each animal is represented by only one sample point with no dependent variable among animals, and the Student's t test is therefore appropriate. The effects were named significant if the p value was smaller than 0.05 (*), 0.01 (**) or 0.001 (***), for a confidence interval of 95, 99 or 99.9%, respectively. Tests to determine sample size were not performed, but our sample sizes were similar to those used in previous publications in the field. All statistical details of experiments can be found in the result section and in the figure legends.

DATA AND CODE AVAILABILITY

Data and custom code supporting the current study have not been deposited in a public repository but are available from the Lead Contact on request.